IEEE Photonics Journal
An IEEE Photonics Society Publication

Open Access

All-Optical Low-Power 2R Regeneration of 10-Gb/s NRZ Signals Using a III-V on SOI Microdisk Laser

Volume 5, Number 6, December 2013

P. Mechet
T. Spuesens
S. Werquin
K. Vandoorne
N. Olivier
J.-M. Fedeli
P. Regreny
D. Van Thourhout
G. Roelkens
G. Morthier

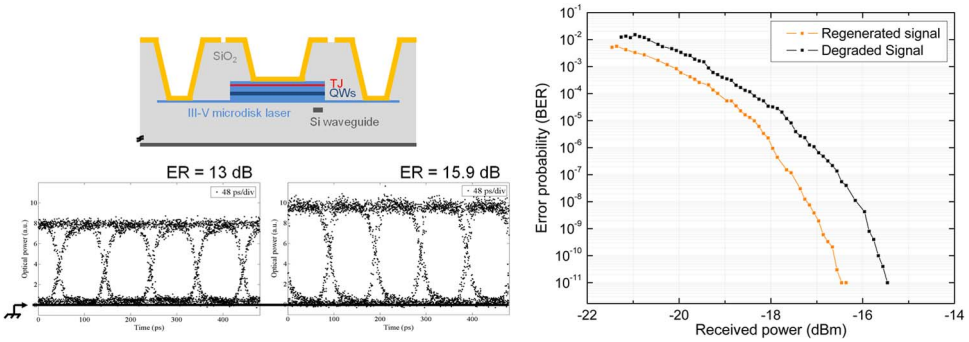

DOI: 10.1109/JPHOT.2013.2287556
1943-0655

All-Optical Low-Power 2R Regeneration of 10-Gb/s NRZ Signals Using a III-V on SOI Microdisk Laser

P. Mechet,[1] T. Spuesens,[1] S. Werquin,[1] K. Vandoorne,[1] N. Olivier,[2] J.-M. Fedeli,[2] P. Regreny,[3] D. Van Thourhout,[1] G. Roelkens,[1] and G. Morthier[1]

[1]Photonics Research Group—Department of Information Technology (INTEC), Ghent University—IMEC, 9000 Ghent, Belgium
[2]CEA-Leti, 38054 Grenoble, France
[3]Institut des Nanotechnologies de Lyon INL-UMR5270, CNRS, Université de Lyon, Ecole Centrale de Lyon, 69134 Écully, France

DOI: 10.1109/JPHOT.2013.2287556

Manuscript received September 9, 2013; revised October 17, 2013; accepted October 18, 2013. Date of publication October 28, 2013; date of current version November 1, 2013. This work was supported by the FP7-ICT European Projects HISTORIC and WADIMOS, by the BOF-Methusalem Grant, and by the Interuniversity Attraction Poles program of the Belgian Science Policy Office under Grant IAP VII/35 "photonics@be." Corresponding author: P. Mechet (e-mail: pauline.mechet@intec.ugent.be).

Abstract: We demonstrate an all-optical low-power 2R regenerator of 10-Gb/s non-return-to-zero data based on a 10-μm-diameter electrically pumped microdisk laser, which is heterogeneously integrated onto the silicon-on-insulator platform and processed in a CMOS pilot line. The scheme results in BER improvement 8and works for submilliwatt-level input signals. The laser operates in the continuous-wave regime, and it is single mode at room temperature and consumes 6 mW of electrical power. Its regeneration capability is investigated in simulations and experimentally demonstrated.

Index Terms: Silicon photonics, heterogeneous III-V integration, microdisk lasers, bonding, regeneration, all-optical signal processing.

1. Introduction

With the growth of Internet-based services, the telecommunication industry is faced with an ever increasing need for bandwidth. Electronic interconnects are fundamentally limited in the achievable bandwidth–distance product, and therefore, an alternative solution needs to be found. Its realization should also be CMOS compatible in order to be cost effective. With the advances in photonic integration technology, an integrated optical solution has become feasible. Optical wavelength-division-multiplexed (WDM) network links were already able to fulfill the bandwidth capacity requirements in the past. However, due to the increasing demand, the logical next step in optical network evolution will be to implement the routing and switching in the optical domain. As systems consist of an increasing number of components working together, the amount of data that needs to be sent across a chip and between different system components increases as well. A major concern here is the accumulation of noise, which severely limits the cascadability of optical network nodes [1]. Different techniques have been proposed for 2R regeneration (re-amplification, Reshaping), for instance, devices based on interferometric structures such as all-optical SOA-based Mach-Zehnders [2] and devices based on self-phase modulation [3], [4]. The limitations of these schemes are their complex structures, their high power consumption or their ability to only

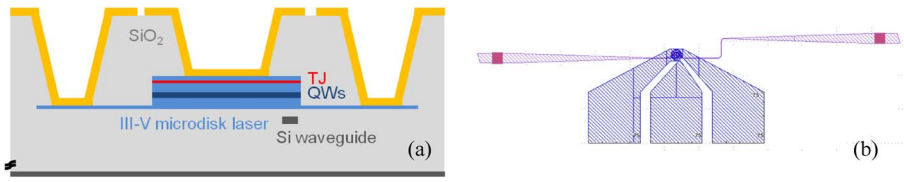

Fig. 1. (a) Schematic representation of the cross-section of the microdisk laser heterogeneously integrated on SOI and embedded in SiO_2. (b) Top view of the designed microdisk laser. The SOI waveguide ends on both sides with a fiber-coupler.

regenerate return-to-zero (RZ) signals. Stand-alone semiconductor optical amplifiers (SOAs) are more attractive in terms of switching, gating, wavelength conversion, and regeneration due to their optical gain, their strong nonlinear behavior, and their integrability in photonic circuits. Error and pattern dependence-free 40 Gb/s 3R regeneration (re-amplification, reshaping, re-timing) has been demonstrated using a single SOA in a delayed-interference configuration [5]. Bistable semiconductor ring lasers have proven to be good candidates for all-optical signal regeneration (2R) and re-timing [6]. In the 2R operation, the extinction ratio (ER) of the optical data pulse is significantly improved when the input ER is as low as 1 dB. Passive signal regeneration based on a membrane InP switch has been reported [7]. Because of the high confinement of light in the active region of the membrane switch, the device acts as a saturable absorber with a highly non-linear response. Improvement in the ER and regenerator operation up to 5 Gb/s have both been shown. Finally, a broadband optical colorless 2R regenerator based on a single distributed feedback laser is also able to regenerate 25 Gb/s non-return-to-zero (NRZ) signals, as reported in [8].

Semiconductor microring or microdisk lasers are suitable as bistable lasers for optical switching or signal processing applications [9]. Using heterogeneous integration, their incorporation in photonics integrated circuits has been made relatively easy. Microring lasers with very low threshold currents have been demonstrated, making these lasers good candidates for light sources for, e.g., on-chip optical interconnects [10]. Microdisk lasers are moreover very versatile devices, used as wavelength converters [11], modulators, and resonant photodetectors [12], all with minimal power consumption.

In this paper, we present a new signal processing application of the microdisk laser, used as regenerator. We demonstrate the regeneration of 10 Gb/s NRZ signals based on a microdisk laser heterogeneously integrated on the Silicon-On-Insulator (SOI) platform and fabricated in a CMOS pilot-line. The regenerator only requires 6 mW of operational power and works for sub-milliwatt level input signals, which makes the scheme simpler and more power efficient than opto-electronic regeneration, that typically requires several watts.

2. Device Design and Integration Technology

The device fabrication in the CMOS pilot-line relies on the molecular bonding of a 2-inch wafer of the molecular-beam-epitaxy-grown InP-based heterostructure onto SOI [13], [14]. The 200-mm patterned SOI wafer is planarized by depositing SiO_2 followed by chemical-mechanical polishing (CMP). The SOI circuit consists of narrow SOI waveguides with a width of 800 nm and a height of 220 nm. The SOI waveguides are fabricated in a CMOS fabrication using 248-nm deep ultra-violet (DUV) lithography. The design of the passive SOI circuit for the considered device consists of a 800 nm-wide waveguide, tapered down on both sides to a 450 nm-wide waveguide. The 450 nm-wide waveguides themselves are tapered up to shallow-etch (etch depth: 70 nm out of the 220 nm) grating couplers (GCs) used to collect the laser emission from the microdisk out of the chip in a single-mode optical fiber [15]. The fiber GCs are optimized for operation at 1.55 μm.

The device is schematically depicted in Fig. 1. The unprocessed III-V wafer, which is coated with a thin layer of SiO_2, is bonded top side down on the patterned SOI wafer by means of molecular bonding. The two levels are then separated by a 130 nm-thick layer of SiO_2 $(n = 1.47)$, allowing evanescent coupling to the underlying waveguide. After the bonding process, the InP substrate is removed so that only the desired epitaxial structure remains. Alignment markers for subsequent

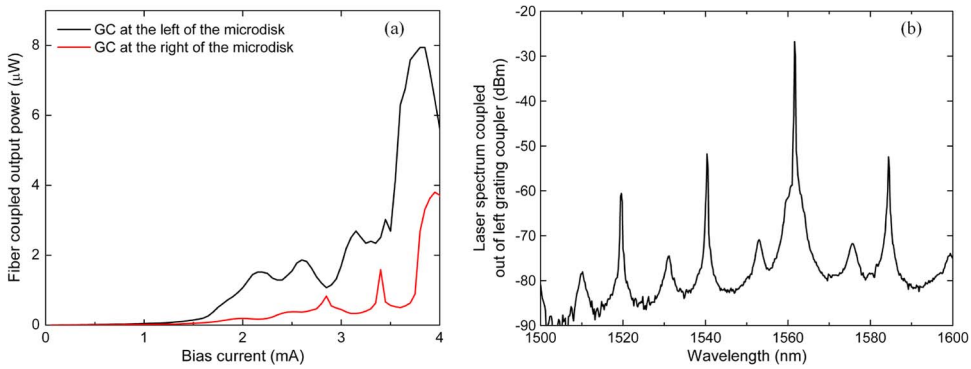

Fig. 2. (a) LI characteristic of a microdisk laser with a diameter of 10 μm. The optical power coupling out of the grating couplers on both sides of the waveguide is simultaneously collected in optical fibers. (b) Single-mode operation of a 10-μm diameter microdisk laser under continuous-wave bias (at 4 mA).

processing are defined in the Si layer relative to the waveguide structures. This allows the accurate alignment of microdisk lasers with respect to the waveguides. The coupling section between the microdisk and the passive circuit is in the middle of the 800 nm-wide waveguide. The microdisk lasers have a diameter of 10 μm and consist of 483 nm thin disk cavity on top of a 100 nm thin InP bottom contact layer. The active layers consist of three compressively strained InAsP quantum wells emitting around 1530 nm and are surrounded by an n-doped layer at the bottom and a p-doped layer at the top to form the diode structure. A tunnel junction is implemented on the p-side such that an n-type contact layer can be used instead of a heavily doped p-type contact layer, in order to reduce optical absorption significantly. The tunnel junction also ensures uniform current injection over the disk [16]. The standard III-V processing steps comply with a 200-mm wafer scale CMOS environment. In particular, 248-nm DUV lithography is used to accurately define the III-V structures. All etching, oxide isolation layer deposition, and metallization steps are performed at 200-mm wafer scale. Two dry etching steps are needed, one to define the disk cavity and another one to make the disk laser bottom contact area. SiO_2 is deposited as cladding layer, and a CMP step is performed to planarize the surface. The low refractive index of the material ensures good optical confinement of the laser light in the microdisk laser. It also reduces the optical losses induced by the metallic top contact as the distance between the optical mode and the metal can be made large enough. To be able to contact the devices, all vias are etched in a single step where the III-V materials are used as an etch stop. The standard Ti/Pt/Au contacts cannot be used as gold is not allowed in a CMOS environment. Therefore, a CMOS compatible Ti/TiN/AlCu (10/40/1000 nm) metal stack is used [17] and demonstrates very good specific contact resistances [18]. The 1 μm-thick contact also serves as a heat sink as it improves the heat dissipation under continuous-wave bias. Above threshold, the laser emission from the microdisk is coupled to the TE mode of the waveguide and is simultaneously collected out of both GCs in optical fibers positioned at 10° angle in order to maximize the collection at 1.55 μm.

3. Static Microdisk Laser Performance

The microdisk laser considered here has a diameter of 10 μm, and the emitted light evanescently couples to one underlying waveguide. The light-current (LI) characteristic of the microdisk laser, measured simultaneously at the two ends of the SOI waveguide, is depicted in Fig. 2(a). This measurement was undertaken under continuous wave operation at room temperature.

When the threshold current of 1.6 mA is surpassed, the microdisk laser is unidirectional. The asymmetry in field reflectivity on both sides of the waveguide leads to different back reflection levels in the laser cavity, as will be discussed below. This difference is responsible for the difference in output power between the two sides. The maximum optical power collected in the fiber is 8 μW (this corresponds to 40 μW in the silicon waveguide). Fig. 2(b) shows the output power spectrum of the

biased microdisk laser (under continuous-wave bias at 4.0 mA) which illustrates single-mode lasing at 1561.6 nm. The free-spectral range of the laser is 22 nm, and a side-mode suppression ratio of 25 dB is measured in Fig. 2(b).

4. Simulation of the Regeneration Behavior

We formulate the rate equations for the fields in the microdisk laser in terms of two counterpropagating whispering gallery modes with electric fields E^+, propagating in the clockwise (CW) direction, and E^-, propagating in the counterclockwise (CCW) direction, as [19], [20]

$$\frac{dE^+}{dt} = \frac{1}{2}(1 - j\alpha)\left(G^+ - \frac{1}{\tau_p}\right)E^+ + KE^- \tag{4.1}$$

$$\frac{dE^-}{dt} = \frac{1}{2}(1 - j\alpha)\left(G^- - \frac{1}{\tau_p}\right)E^- + KE^+. \tag{4.2}$$

The model includes internal losses in the cavity and losses due to outcoupling through the photon-lifetime parameter τ_p. The parameter α is the linewidth enhancement factor that accounts for variations in refractive index due to carrier fluctuations in the semiconductor medium. G is the modal gain factor which will be described further, and $K = K_d + jK_c$ represents an explicit linear coupling rate between the two modes where K_d is the dissipative coupling and K_c the conservative coupling. This coupling term describes the coupling between the CW and CCW modes due to sidewall roughness.

For the carrier density rate equation, we find

$$\frac{dN}{dt} = \frac{I}{qV} - \frac{N}{\tau_c} - G^+|E^+|^2 - G^-|E^-|^2. \tag{4.3}$$

I denotes the injected current, and τ_c is the carrier lifetime. The two other terms take into account the carrier depletion due to stimulated emission. The gain experienced in a semiconductor material decreases for high optical intensity. This is due to gain suppression. Gain suppression takes place even when the total carrier density N is constant and reflects the reduction of "resonant carriers" due to carrier heating and spectral hole burning. To account for this effect, the modal gain can be written as

$$G^+ = \Gamma g_0 \upsilon_g (N - N_0)\left(1 - \varepsilon_s|E^+|^2 - \varepsilon_c|E^-|^2\right) \tag{4.4}$$

$$G^- = \Gamma g_0 \upsilon_g (N - N_0)\left(1 - \varepsilon_s|E^-|^2 - \varepsilon_c|E^+|^2\right) \tag{4.5}$$

where ε_s reflects the self-gain suppression and ε_c the cross-gain suppression. The confinement factor Γ is due to the limited height of the active multi-quantum well. N_0 is the transparency carrier density, g_0 is the differential gain, and υ_g is the group velocity in the microdisk laser. Strain in the quantum wells has a large impact on the band structure of the active material and can have beneficial effects on the gain, by reducing the transparency carrier density and/or improving the differential gain.

Calculations have shown that $\varepsilon_c = 2\varepsilon_s$ [21], [22]. The cross-gain suppression ε_c will therefore break the symmetry and enforce unidirectional operation of the laser. The gain suppression is, however, only significant when the photon density is high. This means that, at lower output powers, normally, a bidirectional regime will be present. Table 1 summarizes the parameters implemented in the numerical solving of the above set of equations. The simulation is performed at the resonance wavelength of the microdisk laser (1561.6 nm). The value for the linear coupling coefficient K is chosen so that the simulation matches the experimental results presented in Section V of this paper.

In order to model the asymmetry in reflection from both sides of the waveguide, an extra term is explicitly added to the rate equations in Eq. (4.6) and (4.7) to calculate the fields propagating in the CW direction and the CCW direction, respectively. The normalized field reflectivity from the bus

TABLE 1

Parameters considered for the simulation of the regeneration behavior of a microdisk laser

Symbol	Name of the parameter	Value	Unit	Reference
R	Microdisk radius	5	μm	
τ_p	Photon lifetime	0.47	ps	[23]
τ_c	Carrier lifetime	600	ps	[23]
α	Linewidth enhancement factor	4		
v_g	Group velocity in the microdisk laser	3E8/3.4	$m.s^{-1}$	[23]
ε_s	Self-gain suppression	1.1E-17	cm^3	
ε_c	Cross-gain suppression	2 x 1.1E-17	cm^3	
g_0	Differential gain	7E-17	cm^2	
N_0	Transparency carrier density	1E18	cm^{-3}	[23]
κ	Field coupling disk-waveguide	0.29		
T_1	Normalized field reflectivity from the right side of the waveguide	$0.25\|\kappa\|^2$	s^{-1}	
T_2	Normalized field reflectivity from the left side of the waveguide	0	s^{-1}	
K	Symmetric coupling between the two modes due to sidewall roughness	5.6E-5 +2.8E-4j	s^{-1}	
RR	Spontaneous emission amplitude	2	s^{-1}	
P_{in}	Average power of the injected optical pulses in the microdisk laser	0.35	mW	

waveguide is implemented with a coefficient $T_i = r_i|\kappa|^2$, where r_i represents the field reflection coefficient from the left/right side of the silicon waveguide measured at the microdisk/bus waveguide interface, and $|\kappa|^2$ is the power coupling coefficient between the silicon waveguide and the microdisk laser. Also, in Eqs. (4.6) and (4.7), the spontaneous emission of the microdisk laser is implemented in two electric fields $E_{noise1}(t)$ and $E_{noise2}(t)$ where $E_{noise} = RR.n.e^{2j\pi n'}$, with RR representing the spontaneous emission amplitude and n and n' random numbers between 0 and 1. Finally, in Eq. (4.7), the calculation of the CCW field takes the injection of optical pulses on the left side of the waveguide into account (represented by E_{in}). That is

$$\frac{dE^+}{dt} = \frac{1}{2}(1 - j\alpha)\left(G^+ - \frac{1}{\tau_p}\right)E^+ + KE^- + E_{noise1} + T_1E^- \tag{4.6}$$

$$\frac{dE^-}{dt} = \frac{1}{2}(1 - j\alpha)\left(G^- - \frac{1}{\tau_p}\right)E^- + KE^+ + E_{noise2} + T_2E^+ + \kappa\frac{v_g}{2\pi R}E_{in}. \tag{4.7}$$

We simulate the injection of a noisy 10 Gb/s pseudo-random bit-sequence (PRBS) in the waveguide, along the CCW direction of propagation. The microdisk laser in the simulation is operated at 4 mA under continuous-wave bias and is originally lasing in the CW direction. Gaussian white noise is added to the electrical field of the input signal, both in the logical "1" level and in the logical "0" level. The input signal is then filtered using a band-pass filter with a bandwidth of 61 GHz. The average input power coupled to the microdisk is then 0.35 mW. The optical power of the noisy and filtered input pattern in the waveguide before the microdisk laser is plotted in Fig. 3(a). In the simulation, the optical power traveling in the cavity and in the bus waveguide is obtained from a conversion of the photon density $|E|^2$ (implemented in the simulation in cm^{-3} as $P = |E|^2\hbar\omega v_g A_{eff}$, where A_{eff} is the effective area of the optical mode. The resulting eye diagram is depicted in Fig. 3(b).

We calculate the amplitude of the field at the output of the microdisk laser. Fig. 4(a) shows what happens when the 10 Gb/s data stream is injected from the left side (at $t = 0$). The field propagating on the right side of the waveguide [blue trace in Fig. 4(a)] consists of the transmitted input field and of the CCW laser emission of the microdisk laser coupled to the waveguide. The destructive interference between the CCW laser emission of the microdisk laser and the transmitted input field is taken into account in the simulation. The field propagating on the left side of the waveguide [green trace in Fig. 4(a)] consists of the CW laser emission of the microdisk laser coupled to the waveguide. From $t = 0$ to $t = 300$ ps, the microdisk laser threshold is not yet reached. Only the

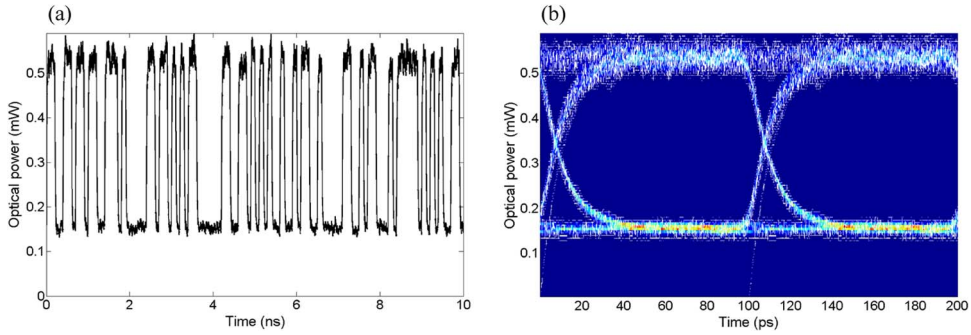

Fig. 3. (a) Degraded pseudo-random-bit-sequence (PRBS) in the waveguide after filtering with a 61 GHz band-pass filter: Gaussian white noise is visible on the trace of the optical power of the input signal. (b) Resulting eye diagram of the degraded and filtered signal in the waveguide before the microdisk

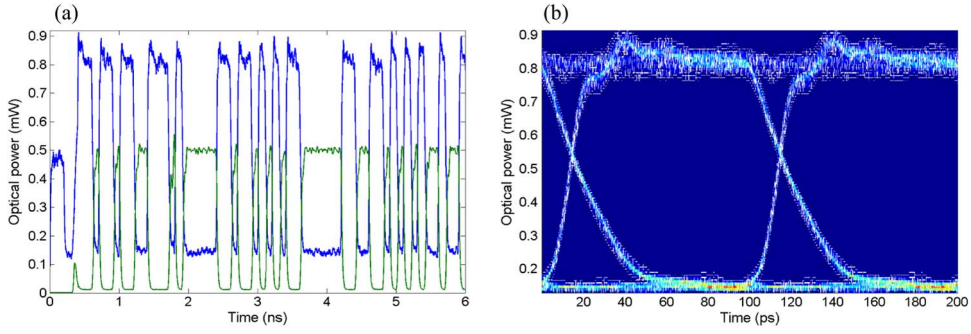

Fig. 4. (a) Optical powers at the output of the microdisk laser, in the waveguide, after filtering with a 61 GHz band-pass filter. Above threshold, the microdisk is lasing in the CW dominant state (green) ($t < 400$ ps), but as soon as an optical pulse is injected on the left side of the waveguide, the microdisk switches to lase in the CCW dominant state (blue). After the pulse has passed through, the microdisk laser switches back to the CW mode (green). (b) Resulting eye diagram of the regenerated and filtered signal in the waveguide after the microdisk laser.

transmitted input field is measured on the right side of the waveguide. At $t = 300$ ps, we observe that the microdisk laser starts lasing in the CW dominant state, in which the CCW mode is suppressed. The power measured on the left side of the SOI is increasing. From $t = 400$ ps and for the rest of the PRBS sequence, we see that the injected external pulses couple into the microdisk cavity. As the injected pulses are strong enough, they switch the laser to operate in the CCW mode. In this case, the power on the left side of the SOI waveguide becomes low. But after the pulses have passed through, the asymmetry in the reflectivity from the right side of the bus waveguide forces the microdisk laser to switch back to the CW mode. To suppress transient oscillations of the laser, we also implement a band-pass filter with a bandwidth of 61 GHz at the right output of the microdisk laser. The eye diagram of the optical power in the waveguide after the bandpass filter is depicted in Fig. 4(b). It is plotted above threshold of the microdisk laser. The optical power then consists of the transmitted input power and of the CCW laser emission of the microdisk laser coupled to the waveguide. The noise level of the signal after the microdisk laser is reduced compared to the noise level of the input PRBS. The ER measurement is carried out by measuring the logical "0" and "1" levels of the data waveform. The calculated ER of the eye diagram of the input signal [Fig. 3(b)] is 4.7 dB, while the calculated ER of the eye diagram of the regenerated signal [Fig. 4(b)] is 7.3 dB.

We simulate the ER of the regenerated signal in the waveguide as a function of the input pulse power. The regenerated signal consists of the transmitted input field and of the CCW laser emission of the microdisk laser coupled to the waveguide. The parameters for this simulation are identical to

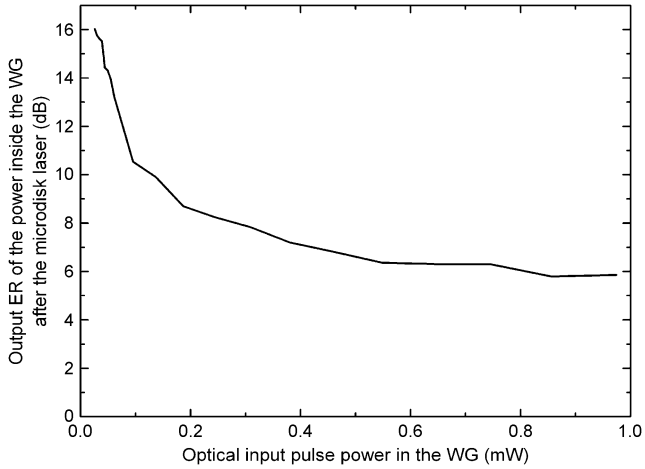

Fig. 5. Evolution of the ER of the optical power in the waveguide after regeneration as a function of the input pulse power in the waveguide.

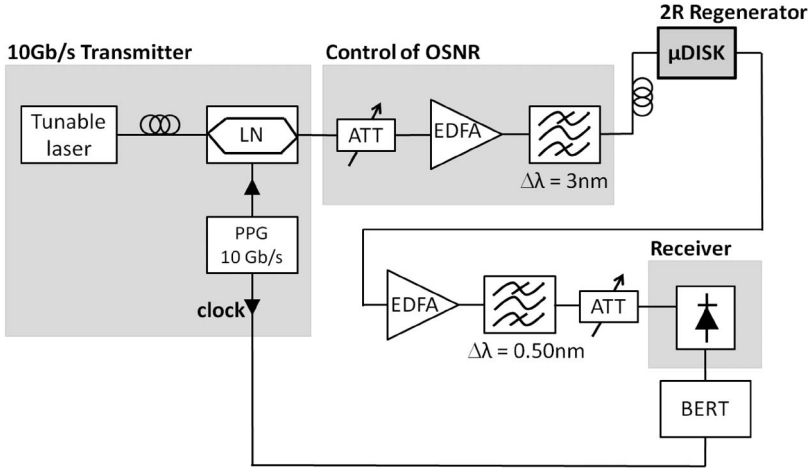

Fig. 6. Schematic of the setup (LN: lithium-niobate modulator; PPG: Pulse Pattern Generator; ATT: attenuator; EDFA: erbium-doped fiber-amplifier; μDISK: microdisk laser; BERT: bit error rate tester).

the ones listed in Table 1. The microdisk laser is still operated at 4 mA under continuous-wave bias. The ER of the PRBS signal is kept constant and equal to 5.6 dB. In Fig. 5, it is clear that, for low input pulse powers (lower than 0.1 mW in the waveguide), the ER of the signal after the microdisk laser is greatly improved. The influence of the laser emission of the microdisk laser on the eye diagram of the regenerated signal is strong. For higher input pulse powers, the contribution of the transmitted input field in the regenerated signal is stronger and the effect of the laser emission from the microdisk on the regeneration is less significant. The advantage of the regenerator lies in the fact that it is effective for sub-milliwatt input signals, which makes it more power efficient than opto-electronic regeneration.

5. Regenerator Demonstration: Results at 10 Gb/s

For the experiment, we use the setup depicted in Fig. 6. Light from a tunable laser source at the resonance wavelength of the microdisk laser (1561.6 nm) is sent through a modulator, which is driven by a 10 Gb/s pulse pattern generator (PPG). The PPG generates a PRBS of 2^{31}-1 bits. We

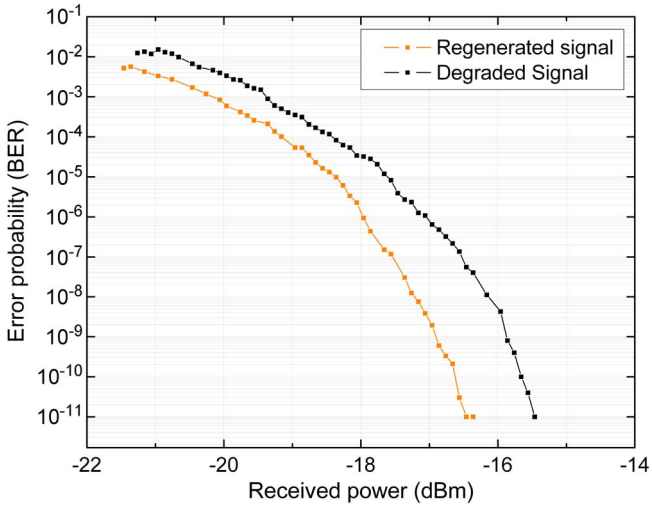

Fig. 7. BER measurement results with and without 2R regeneration at 10 Gb/s. The average power of the degraded signal coupled to the microdisk laser is in the sub-milliWatt range.

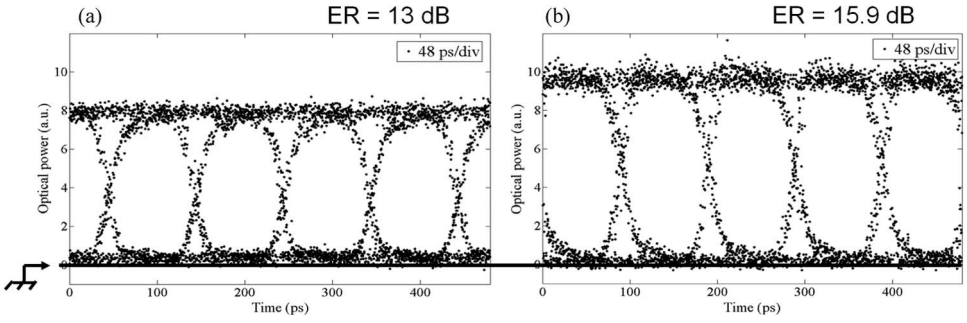

Fig. 8. (a) Eye diagram of the degraded signal. (b) Eye diagram of the regenerated signal.

use polarization controlling wheels after the laser source as the modulator only works in TE mode. The original signal is being attenuated, amplified using an erbium-doped fiber amplifier (EDFA), and filtered with a 3 nm optical band-pass filter to decrease the optical signal-to-noise ratio. The resulting signal has an average power of 3.5 dBm after degradation and is injected with an optical fiber under a 10° angle into the waveguide through the left GC. Due to a 20% coupling efficiency of the GCs, the optical power coupled to the microdisk laser is in the sub-milliwatt range. Light coupling out of the right GC after the microdisk laser is collected in an optical fiber under a 10° angle. Amplification after the microdisk 2R regeneration was needed to increase the signal power. The optical amplification was implemented in combination with an optical band-pass filter (bandwidth of 0.50 nm) to remove amplified spontaneous emission and to emulate the simulated band-pass filter implemented in the simulations. A variable attenuator is used to change the received optical power on the receiver in order to plot BER-diagrams. The microdisk laser is operated at 4 mA under continuous-wave bias.

The regenerative capabilities of the regenerator under dynamic operation at 10 Gb/s are demonstrated. Fig. 7 shows the BER measurement results of the degraded signal and the regenerated signal. To measure the BER of the degraded signal, the modulated light out of the 3 nm optical band-pass filter is directly sent to the second EDFA. Fig. 8(a) and (b) show the eye diagrams with and without the 2R regenerator. Clearly, the signal is regenerated. An improvement in the ER is demonstrated. For an input signal with a 13 dB-ER, a 2.9 dB-improvement in ER is measured. The

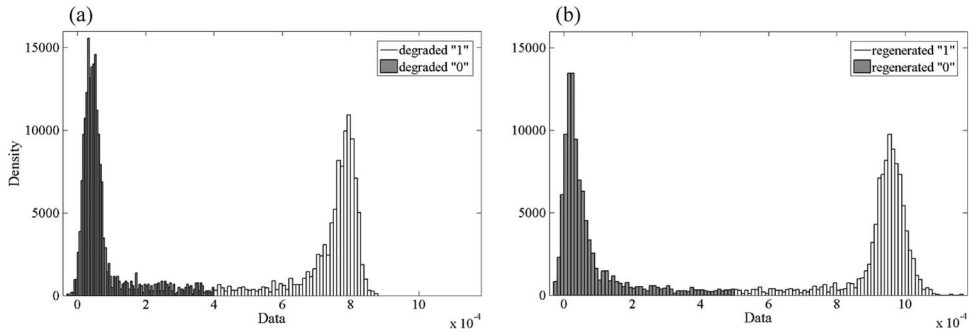

Fig. 9. Distributions of the logical "1" and the logical "0" levels from (a) the eye diagram of the degraded signal and (b) the eye diagram of the regenerated signal (from Fig. 8).

relatively low experimental ER improvement is due to the presence of the EDFA before the photoreceiver and to a high receiver noise. The amplified spontaneous emission from the EDFA considerably increases the level of the logical "0." The regeneration is also visible in Fig. 9 where the distributions of the logical "0" and logical "1" levels from the two eye diagrams are plotted. The noise is significantly reduced after regeneration, even though we still suffer from the amplified spontaneous emission from the EDFA located before the receiver. The eye becomes more open after the 2R regenerator. Less data points are present between the two logical levels on the distribution related to the regenerated signal [Fig. 9(b)] than on the distribution related to the degraded one [Fig. 9(a)]. The distribution of logical "1" level is also narrower after regeneration. We demonstrate an improvement in the Q-factor, from 3.93 for the eye of the degraded signal [Fig. 8(a)] to 4.24 for the eye of the regenerated signal [Fig. 8(b)].

6. Conclusion

A new concept for 2R regeneration is proposed using a microdisk laser. Improvement in ER and noise reduction have been experimentally demonstrated. We reported bit error rate improvement in 10 Gb/s NRZ signals. We explain the relatively low re-amplification of the signal after the microdisk laser by the low photon lifetime in the cavity. Simulations demonstrate optical output powers in the milli-watt range in the waveguide after the microdisk laser when the photon lifetime is increased to a few picoseconds. Improving the etching process of the microdisk (improvement in the sidewall roughness) will increase the photon lifetime and allow the combination of the noise reduction to a stronger re-amplification of the signal. The advantage of the regenerator lies in the fact that it is effective for sub-milliwatt input signals and consumes 6 mW of operational power. The regenerators presented in [2], [5], and [8] all require optical input powers of several milli-watts and are biased above 100 mA. This CMOS compatible scheme is promising for all-optical regeneration in future optical networks.

References

[1] D. A. B. Miller, "Are optical transistors the logical next step?" *Nat. Photon.*, vol. 4, no. 1, pp. 3–5, Jan. 2010.
[2] D. Wolfson, A. Kloch, T. Fjelde, C. Janz, B. Dagens, and M. Renaud, "40-Gb/s all-optical wavelength conversion, regeneration, and demultiplexing in an SOA-based all-active Mach-Zehnder interferometer," *IEEE Photon. Technol. Lett.*, vol. 12, no. 3, pp. 332–334, Mar. 2000.
[3] P. V. Mamyshev, "All-optical data regeneration based on self-phase modulation effect," in *Proc. 24th Eur. Conf. Opt. Commun.*, Madrid, Spain, 1998, pp. 475–476.
[4] M. Rochette, L. B. Fu, V. Ta'eed, D. J. Moss, and B. J. Eggleton, "2R optical regeneration: An all-optical solution for BER improvement," *IEEE J. Sel. Topics Quantum Electron.*, vol. 12, no. 4, pp. 736–744, Jul./Aug. 2006.
[5] J. Leuthold, B. Mikkelsen, R. E. Behringer, G. Raybon, C. H. Joyner, and P. A. Besse, "Novel 3R regenerator based on semiconductor optical amplifier delayed-interference configuration," *IEEE Photon. Technol. Lett.*, vol. 13, no. 8, pp. 860–862, Aug. 2001.
[6] B. Li, M. Irfan Memon, G. Mezosi, Z. Wang, M. Sorel, and S. Yu, "Characterization of all-optical regeneration potentials of a bistable semiconductor ring laser," *J. Lightwave Technol.*, vol. 27, no. 19, pp. 4233–4239, Oct. 2009.

[7] M. Tassaert, H. J. S. Dorren, G. Roelkens, and O. Raz, "Passive InP regenerator integrated on SOI for the support of broadband silicon modulators," *Opt. Exp.*, vol. 20, no. 10, pp. 11 383–11 388, May 2012.
[8] K. Huybrechts, T. Tanemura, K. Takeda, Y. Nakano, R. Baets, and G. Morthier, "All-optical 2R regeneration using the hysteresis in a distributed feedback laser diode," *IEEE J. Quantum Electron.*, vol. 16, no. 5, pp. 1434–1439, Sep./Oct. 2010.
[9] L. Liu, R. Kumar, K. Huybrechts, T. Spuesens, G. Roelkens, E.-J. Geluk, T. de Vries, P. Regreny, D. Van Thourhout, R. Baets, and G. Morthier, "An ultra-small, low-power, all-optical flip-flop memory on a silicon chip," *Nat. Photon.*, vol. 4, no. 3, pp. 182–187, Mar. 2010.
[10] D. Liang, M. Fiorentino, S. Srinivasan, S. T. Todd, G. Kurczveil, J. E. Bowers, and R. G. Beausoleil, "Optimization of hybrid silicon microring lasers," *IEEE Photon. J.*, vol. 3, no. 3, pp. 580–587, Jun. 2011.
[11] R. Kumar, T. Spuesens, P. Mechet, P. Kumar, O. Raz, N. Olivier, J.-M. Fedeli, G. Roelkens, R. Baets, D. Van Thourhout, and G. Morthier, "Ultra-fast and bias-free all-optical wavelength conversion using III-V on silicon technology," *Opt. Lett.*, vol. 36, no. 13, pp. 2450–2452, Jul. 2011.
[12] J. Hofrichter, T. Morf, A. La Porta, O. Raz, H. J. S. Dorren, and B. J. Offrein, "A single InP-on-SOI microdisk for high-speed half-duplex on-chip optical links," *Opt. Exp.*, vol. 20, no. 26, pp. 365–370, Dec. 2012.
[13] J. B. Lasky, "Wafer bonding for silicon-on-insulator technologies," *Appl. Phys. Lett.*, vol. 48, no. 1, pp. 78–80, Jan. 1986.
[14] M. Kostrzewa, L. Dicioccio, M. Zussy, J. Roussin, J. Fedeli, N. Kernevez, P. Regreny, C. Lagaheblanchard, and B. Aspar, "InP dies transferred onto silicon substrate for optical interconnects application," *Sens. Actuators A, Phys.*, vol. 125, no. 2, pp. 411–414, Jan. 2006.
[15] F. Van Laere, G. Roelkens, M. Ayre, J. Schrauwen, D. Taillaert, D. Van Thourhout, T. F. Krauss, and R. Baets, "Compact and highly efficient grating couplers between optical fiber and nanophotonic waveguides," *J. Lightwave Technol.*, vol. 25, no. 1, pp. 151–156, Jan. 2007.
[16] J. Van Campenhout, P. Rojo Romeo, D. Van Thourhout, C. Seassal, P. Regreny, L. Di Cioccio, J.-M. Fedeli, and R. Baets, "Design and optimization of electrically injected InP-based microdisk lasers integrated on and coupled to a SOI waveguide circuit," *J. Lightwave Technol.*, vol. 26, no. 1, pp. 52–63, Jan. 2008.
[17] L. Grenouillet, A. Bavencove, T. Dupont, J. Harduin, P. Philippe, P. Regreny, F. Lelarge, K. Gilbert, P. Grosse, and J. Fedeli, "CMOS compatible contacts and etching for InP-on-silicon active devices," in *Proc. 6th IEEE Int. Conf. GFP*, 2009, pp. 196–198.
[18] T. Spuesens, F. Mandorlo, P. Rojo-Romeo, P. Regreny, N. Olivier, J. M. Fedeli, and D. Van Thourhout, "Compact integration of optical sources and detectors on SOI for optical interconnects fabricated in a 200 mm CMOS pilot line," *J. Lightwave Technol.*, vol. 30, no. 11, pp. 1764–1770, Jun. 2012.
[19] M. Sorel, G. Giuliani, A. Scire, R. Miglierina, S. Donati, and P. J. R. Laybourn, "Operating regimes of GaAs-AlGaAs semiconductor ring lasers: Experiment and model," *IEEE J. Quantum Electron.*, vol. 39, no. 10, pp. 1187–1195, Oct. 2003.
[20] T. Numai, "Analysis of signal voltage in a semiconductor ring laser gyro," *IEEE J. Quantum Electron.*, vol. 36, no. 10, pp. 1161–1167, Oct. 2000.
[21] E. J. D'Angelo, E. Izaguirre, G. B. Mindlin, G. Huyet, L. Gil, and J. R. Tredicce, "Spatiotemporal dynamics of lasers in the presence of an imperfect O(2) symmetry," *Phys. Rev. Lett.*, vol. 68, no. 25, pp. 3702–3705, Jun. 1992.
[22] M. Sargent, "Theory of a multimode quasi-equilibrium semiconductor-laser," *Phys. Rev. Lett. A, At. Mol. Opt. Phys.*, vol. 48, no. 1, pp. 717–726, Jul. 1993.
[23] J. Van Campenhout, "Thin-film microlasers for the integration of electronic and photonic integrated circuits," Ph.D. dissertation, Ghent Univ., Ghent, Belgium, 2007.